

Author Version : Palaeogeography, Palaeoclimatology, Palaeoecology, vol.516; 2019; 22-34

Impact of the Indian Summer Monsoon variability on the source area weathering in the Indo-Burman ranges during the last 21 kyr – A sediment record from the Andaman Sea

Tyson Sebastian¹, B. Nagender Nath^{1*}, M. Venkateshwarlu², Pavan Miriyala², Archana Prakash¹, P. Linsy¹, M. Kocherla¹, Armoury Kazip¹ and A.V.Sijinkumar³,

¹CSIR- National Institute of Oceanography, Dona Paula, Goa, India, 403004

²CSIR – National Geophysical Research Institute, Uppal Road, Hyderabad, India, 500007

³Department of Geology, Central University of Kerala, Kasaragod, India

*Corresponding author email: nagendernath@yahoo.com

Abstract

The paleomonsoonal variations and their impact on the weathering patterns in the source regions of sediments of the Andaman Sea were investigated from a 21 kyr sedimentary record using environmental magnetic, clay mineralogical and geochemical techniques. The sediment provenance of the study area determined from the geochemical discrimination diagrams and available ϵ_{Nd} records indicates that the Western Andaman Sea receives a considerable contribution from the Indo-Burman Ranges (IBR) and local sources compared to the central and eastern Andaman Sea. The results illustrate a strong Indian Summer Monsoon (ISM) during the late glacial (16 – 13 kyr), early (10.5 – 8.5 kyr) and middle Holocene (5 – 3.5 kyr) and a weak ISM during the Younger Dryas (12.9 – 11.7 kyr) and late Holocene (3.5 – 0 kyr) periods. The mineral magnetic grain size parameters ($\chi_{ARM}/SIRM$, $SIRM/\chi_{LF}$, χ_{ARM}/χ_{LF}) show finer grain sizes during the strong ISM periods indicating the increased chemical weathering while cold and dry periods are marked by an increase in magnetic grain size indicating the shift from chemical to physical weathering in the source regions. The results from our study are in agreement with the global and local records of paleoclimate and weathering and exhibit a close correlation with the solar insolation data suggesting the major role played by the solar forcing on the ISM variability.

Keywords: Environmental Magnetism, Chemical Weathering, Paleomonsoon, Myanmar, Clay Mineralogy, Geochemistry

1. Introduction

The Indian Summer Monsoon system (ISM) is a major part of the Asian Monsoon system and drives the weathering and erosion in the Himalayan and the Burman ranges (Colin et al., 1999; Clift et al., 2008; Rahaman et al., 2009; Miriyala et al., 2017). ISM is responsible for more than 85% of India's annual precipitation and its variations have a large impact on the lives of more than one-sixth of the world population since most of the agricultural activities in the country rely on the monsoons. Therefore, paleomonsoonal reconstructions are of global importance and are essential to better understand the monsoon system of Asia.

The Andaman Back arc Basin is a semi-enclosed basin in the eastern Indian Ocean and is fed mainly by the Myanmar Rivers Irrawaddy, Salween, Sittang and other smaller rivers (Rodolfo, 1969a; Kurian et al., 2008). The changes in the strength of ISM can result in the modification of weathering patterns in the source regions. It is reported that more than 90% of the precipitation in Myanmar and 80% runoff and 87% of sediment discharge from the Irrawaddy-Salween system are controlled by the ISM (Rodolfo, 1969a).

While a number of studies have established the paleoceanography of the Andaman Sea using stable isotopes and foraminiferal proxies (Duplessy, 1982; Naqvi et al., 1994; Ahmad et al., 2000; Rashid et al., 2007; Sijin Kumar, 2011; Sijinkumar et al., 2010, 2016;), only a limited records have shown the monsoon and weathering linkages from the Andaman Sea (Colin et al., 1999, 2006; Awasthi et al., 2014; Ali et al., 2015; Cao et al., 2015; Miriyala et al., 2017). A sediment core named NGHP 01 – 17A was drilled from the Western Andaman Sea (WAS) during the Indian National Gas Hydrate Program (NGHP) using JOIDES Resolution in 2006 (Collett et al., 2008). Ali et al. (2015) have employed the radiogenic Sr, Nd, and Pb isotope compositions of the detrital clay-size fraction and clay mineral assemblages of this sediment core to reconstruct the variability of the South Asian monsoon during the past 60 kyr. Their results indicated that the sources of sediments to the study area did not change considerably during the last 60 kyr due to a spatially stable monsoon. They have constrained the sediment sources to the WAS using radiogenic isotopes and have concluded a major and stable contribution from the Indo - Burman Ranges and Central Myanmar basin to the Andaman Sea through Irrawaddy River with a possible minor contribution from the Andaman Islands.

The above is in contrast with the findings of Awasthi et al. (2014) which stated that since about the early MIS-2 (24 ka), the provenance of WAS sediments changed from an Irrawaddy dominated to an IBA (Indo - Burman – Arakan) - Andaman dominated regime. From a sedimentary record from Central Andaman Sea (SK 168/GC 01), Miriyala et al., (2017) found an increase in

silicate weathering with initiation of interglacial warm climate at ~17.7 ka followed by a major depositional change at 15.5 ka and found provenance shifts during glacial-interglacial periods in the Central Andaman Sea. It is not known if the weathering trends are similar in other watersheds of Myanmar. While the Central Andaman Sea has effectively recorded the weathering changes in the Myanmar water sheds with time (Colin et al., 2006; Miriyala et al., 2017), it is not known if the WAS, which has additional sediment sources including that from local volcanics and islands (Ali et al., 2015; Awasthi et al., 2014; Miriyala et al., 2017), has preserved the weathering signatures.

In this study, an attempt is made to assess the variability of weathering changes since the Last Glacial Maximum (LGM) and its linkage to ISM from a sedimentary record in the WAS using environmental magnetic, clay mineralogical and geochemical proxies at ~135 year time resolution. The core location in this study is the same where the drill core NGHP – 01- 17A was recovered (Collett et al., 2008; Ali et.al., 2015) and very close to Hole U1447 of IODP 353. While the NGHP and IODP records are ideal for studying the geological changes on tectonic timescales, our core was collected with an aim to study the high resolution climatic changes in the WAS on shorter time scales.

2. Geological setting and oceanography of the study area

The Andaman Sea is a confined active back-arc basin in the Northern Indian Ocean covering an area of 80,00,00 km² (Rodolfo, 1969a). It lies along a highly oblique convergent margin between the northeastern moving Australian and/or Indian plate and the nearly stationary Eurasian or Southeast Asian plate (Curry, 2005). The average depth of the Andaman Sea is 1096 m with a rugged volcanic topography in the western part and smooth topography in the eastern side. The tectonic history (Curry, 2005; Kamesh Raju et al., 2004), geology (Rodolfo, 1969b), and hydrography (Babu and Sastry, 1976; Sen Gupta et al., 1981; Varkey et al., 1996) of the Andaman Sea are well established.

The Andaman Sea is characterized by seasonally reversing monsoon (Wyrski, 1973) which results in a cyclonic surface circulation during the summer and spring and an anti-cyclonic circulation throughout the rest of the year (Potemra et al., 1991). The Andaman Sea is connected to the Bay of Bengal through several channels such as the Deep Prepares Channel, Ten Degree Channel and the Great Channel and to South China Sea through Malacca Strait (**Fig. 1**). This results in a similar salinity and temperature distribution in the Eastern Bay of Bengal and the Andaman Sea up to a depth of ~1000 m. The intermediate to deep water circulation between these seas is prevented by shallow sill depth (~1300 m) in the Andaman Sea (Babu and Sastry, 1976). The large fresh water

influx from ISS river systems results in a lowered salinity in the Andaman Sea during the summer monsoon (Varkey et al., 1996).

The principal sources of sediments to the Andaman Sea are the Irrawaddy, Salween and Sittang rivers in Myanmar. In addition to this, Indo – Burman Arakan ranges (IBA), biogenic sources and altered basinal volcanic products also constitute the sediment sources (Kurian et al., 2008). The total annual suspended sediment load of ISS system is potentially as large as 600 million tons (MT) representing 57% of the modern G-B sediment flux (Robinson et al., 2007). The Irrawaddy River drains the Cretaceous to mid-Cenozoic flysch of the western Indo - Burman ranges, Eocene, Miocene and Quaternary sediments of the Myanmar Central Basin, and the Late Precambrian and Cretaceous-Eocene metamorphic, basic, and ultrabasic rocks of the eastern syntaxis of the Himalayas (Robinson et al., 2007). The catchment of Salween and eastern tributaries of the Irrawaddy are mainly Precambrian, Oligocene-Tertiary sedimentary, and acidic and metamorphic rocks of the eastern Shan Plateau (Robinson et al., 2007 and the references therein).

3. Materials and methods

3.1. Sampling

The 1.53 m long gravity core named SSK 50 – GC 3A (hereafter referred as GC 3A) used in this study was collected from the WAS at 10.76°N and 93.10° E from a water depth of 1334 m during the 50th expedition of RV Sindhu Sankalp in May 2013 (**Fig. 1**). The core was subsampled at 1 cm interval.

3.2. Texture and clay mineralogy

The texture of the samples was determined by wet sieving followed by analysis with Laser Particle Size Analyser (LPSA). The sediments were wet sieved using 63 µm mesh and the sand fraction retained on sieves was separated. The <63 µm fraction was made free of calcium carbonate and organic carbon using acetic acid and hydrogen peroxide and then subjected to LPSA analysis (Malvern Mastersizer 2000) to determine the texture of silt-clay sized lithogenic fraction. For clay mineralogy, the clay-sized fraction (<2 µm) was separated using pipette analyses and the suspension was spread evenly on glass slides, and allowed to air-dry. The relative percentages of clay minerals were calculated from the weighted peak area percentages of the major clay minerals from the X-ray diffractograms of the glycolated samples following the semi-quantitative method of Biscaye (1965).

3.3. Environmental magnetic measurements

Environmental magnetic parameters were measured on the freeze dried samples at CSIR – NIO, Goa and CSIR – NGRI, Hyderabad. The major magnetic parameters, ratios, their units and interpretations are tabulated in **Table 1**. The low and high frequency magnetic susceptibility measurements were carried out using Bartington MS2B sensor. Anhyseric remnant magnetization (ARM) was imparted to the samples by applying 100 mT peak alternating field and a 0.05 mT constant bias field using Molspin AF demagnetizer. The ARM intensity was then measured using a spinner magnetometer (JR-6 dual speed spinner magnetometer, AGICO, Brno, Czech Republic). Isothermal remnant magnetization (IRM) was measured using a Molspin pulse magnetizer and saturation isothermal remnant magnetization (SIRM) was measured at a pulse field of 1T (for more details of these analyses refer Sebastian et al., 2017).

3.4. Bulk geochemistry

The geochemical analyses were carried out using XRF and ICP – MS techniques. Major elements were measured in salt and carbonate-free lithogenic fraction using a Wavelength-Dispersive X-ray Fluorescence (XRF-WD; Axios, PANalytical, The Netherlands) at CSIR - NIO, Goa. The decarbonated samples were powdered and 0.55 gm of the sample powder was mixed with Spectromelt® A12 (Merck) flux and borate beads were prepared in a furnace. The standards JMS 1 (Geological Survey of Japan) and MAG 1 (United States Geological Survey) were used for quality control and the accuracy of geochemical analyses was within $\pm 5\%$, while the precision was within $\pm 2\%$ (**Table 2**).

For analyses of trace elements La, Th and Sc the powdered samples were digested using an acid mixture (7:3:1 - HF: HNO₃:HClO₄) in Teflon beakers. All the acids used were of Suprapure (MERCK) grade. The filtered solutions were analyzed using ICP-MS (Thermo Scientific, XSERIES 2, Quadrupole) at CSIR-NIO. The geochemical standards JSD 1 (Geological Society of Japan) and SGR 1b (United States Geological Survey) were used to ensure the quality of the results. The analytical accuracy for the La, Th and Sc was better than $\pm 2\%$ except for Sc of SGR 1b which recorded an accuracy of $\pm 6.7\%$. The precision of the analyses was within $\pm 5\%$. The accuracy and precision data of the geochemical analyses are presented in **Table 3**.

The total carbon content in the sediments was measured on powdered samples using CNS Analyzer (NC Soil analyzer, Thermo Scientific Flash 2000). The total inorganic carbon (TIC) in the sediments was determined using the CO₂ coulometer. Total organic carbon content (C_{org}) was calculated by subtracting TIC from TC values. The accuracy of the analysis was determined using MAG 1 and an NC reference soil sample. Both the accuracy and precision were within $\pm 4\%$.

3.5. Geochronology

For dating, two planktic foraminiferal species *Globigerinoides Ruber* and *Sacculifer* specimens were handpicked from the >125 μm fraction of the sediments at five depths (3-4, 21-22, 51-52, 79-80 and 109-110 cm) within the core. They were then subjected to ^{14}C Accelerator Mass Spectrometry (AMS) dating at Center for Applied Isotope Studies, University of Georgia. The calibration of radiocarbon ages were calibrated to calendar years using the CalPal 2007 program (<http://www.calpal.de>) after applying a standard ocean reservoir correction of 400 years.

4. Results

4.1. Chronological framework

The results from the ^{14}C dating yielded an age of 20.7 ka for the core with an average sedimentation rate of 7.4 cm/kyr which is comparable with the average sedimentation rates of earlier published Andaman Sea records (Colin et al., 1999 - 10.9 cm/kyr during last 74 kyr; Awasthi et al., 2014 - 5.3 cm/kyr during last 23 kyr; Ali et al., 2015 - 11.6 cm/kyr during last 21 kyr; Sijinkumar et al., 2010 - 7 cm/kyr during last 32 kyr). The sedimentation rate remained nearly constant from LGM to mid-Holocene except during the early Holocene (8.5 – 11.5 kyr) where an increase in sedimentation rate was seen. The lowest sedimentation rates (5.2 cm/kyr) were recorded during the late Holocene period (**Fig. 2**). Another record (NGHP 01 – 17A) from the same location has showed a higher sedimentation rate (11.6 cm/kyr) for the last 21 kyr (Ali et al., 2015). The different sedimentation rates in these two records could be due to the differences in coring technique.

4.2. Texture and clay mineralogy

The sediments in GC 3A are predominantly silty clay in texture. The sand, silt and clay content in the sediments vary between 4 – 31 % (average – 12%), 17 – 41% (average – 31%) and 41 – 71% (average – 58%), respectively with coarser grain size during the Holocene compared to deglacial period (**Fig. 3**). The D_{50} values (median size) also record the Holocene coarsening of the grain size. The dominant clay mineral is smectite (46 – 89%, average - 74.5%) followed by kaolinite (4 – 19%, average - 10%), illite (1 – 21%, average -8%) and chlorite (3 – 15%, average -7.5%) (**Fig. 3**). The smectite content shows a gradual downcore increase while illite shows a gradual decrease. Higher kaolinite content is seen during 16 – 13 kyr and mid-Holocene.

4.3. Environmental magnetism

The downcore variations of mineral magnetic parameters of concentration, grain size and mineralogy along with their ratios are shown in **Fig. 4**. The concentration parameters χ_{LF} , χ_{ARM} and SIRM vary between 17 and 53 (average - 25.5, unit – $10^{-8} \text{ m}^3 \text{ kg}^{-1}$), 0.27 – 0.82 (average - 0.57, unit

– $10^{-5} \text{ m}^3 \text{ kg}^{-1}$) and 314 – 1500 (average - 524, unit – $10^{-5} \text{ A m}^2 \text{ kg}^{-1}$) respectively in this core. The concentrations show slightly higher values during 8 – 6 kyr and 12 – 10 kyr compared to deglacial (16 – 13 kyr) and late Holocene (5 – 0 kyr) periods (**Fig. 4**). The values register a peak at 2.2 ka before showing a decreasing trend in the last two millennia. Magnetic grain size parameters, on the other hand show prominent variations throughout the core. The grain size parameters $\chi_{\text{ARM}}/\text{SIRM}$, $\text{SIRM}/\chi_{\text{LF}}$ and $\chi_{\text{ARM}}/\chi_{\text{LF}}$ show finer grain sizes during 10 – 3 kyr (with peaks at 4.5 ka and 9 ka) and 16 – 13 kyr. The higher values of $\chi_{\text{ARM}}/\text{SIRM}$ and $\chi_{\text{ARM}}/\chi_{\text{LF}}$ indicate a finer grain size while a higher value of $\text{SIRM}/\chi_{\text{LF}}$ indicates a coarser grain size (Thompson and Oldfield, 1986). From the SIRM/ARM ratio (average = 23.0) and the bi-plot of $\chi_{\text{FD}}\%$ vs. $\chi_{\text{ARM}}/\text{SIRM}$ (**Fig. 5**), it is clear that the average magnetic grain size of the core falls in the stable single domain (SSD) range (Dearing et al., 1997; Yu and Oldfield, 1993). Magnetic mineralogical parameters S-ratio and Hard IRM (**Table 1**) show a magnetite-dominant mineralogy (average S-ratio - 0.94). The HIRM shows higher values during 3 – 0 kyr and 13 – 11 kyr indicating an increase in the hard magnetic mineral (e.g. hematite) concentration.

4.4. Geochemical parameters

The organic carbon content in the core GC 3A ranges between 0.9 and 2.3% (average - 1.36%) with high values during the 21 – 13 kyr period (1.62%) compared to the Holocene (average - 1.14%) (**Fig.4**). The CaCO_3 content on the other hand, shows a different pattern with highest value during the LGM–deglacial boundary. The carbonate concentration ranges between 20 and 47% (average - 30.3) with lowest values during the early to mid-Holocene and late glacial (19 – 16 kyr) periods (**Fig. 4**). The concentration data of major elements Al_2O_3 , CaO , Na_2O , K_2O and MgO were used in the geochemical interpretation of the core and their concentrations range between 16.5 and 19.98% (average – 18.49%), 1.36 and 2.62% (1.87%), 0.5 and 1.34% (0.81%), 0.8 and 1.76% (0.98%, except for three points which show values 3.3%, 3.7%, 3.2%) and 2.18 and 2.58% (2.35%) respectively. The trace elements La, Th and Sc varied between 12.3 and 23.1 ppm (average - 20), 5.9 and 9.7 ppm (8.3 ppm) and 9.2 and 14.6 ppm (11.6 ppm) respectively with an increasing trend towards the bottom of the core except for the lowest values during the LGM–deglacial boundary at 19.2 ka.

5. Discussion

5.1. Provenance of sediments at GC 3A site

The sources and fluxes of sediments to the Andaman Sea have been the subject of previous studies, with most of them attributing the source to the large catchments of Myanmar Rivers

Irrawaddy, Salween and Sittang (ISS) (Rodolfo, 1969a; Colin et al., 1999; Awasthi et al., 2014; Ali et al., 2015; Miriyala et al., 2017). The contribution from local volcanic sources such as Barren and Narcondam Islands along with other island and hydrothermal sources (Kurian et al., 2008) was usually neglected due to the very high amounts of sediment supply from ISS River system through Martaban Canyon (Ramaswamy et al., 2004). However, the clay mineralogical and geochemical data of WAS sediments presented here show a marked difference from the Irrawaddy source signatures (Garzanti et al., 2016) and suggest sediment input from other sources too (**Fig. 6**). One major indicator for this is the very high smectite content in the GC 3A (average - 74.6%) compared to the surface samples from Myanmar continental shelf (~ 15%) (see also Kurian et al., 2008). Further, high smectite content was found in the WAS sediments (Rodolfo, 1969a, Ali et al., 2015) compared to central and eastern Andaman Sea sediments (Colin et al., 1999; Kurian et al., 2008; Bunsomboonsakul et al., 2012). The high smectite content in the WAS may owe its origin to the weathering of mafic igneous rocks of IBR and Andaman accretionary prism. This interpretation is supported by the clay mineral distribution maps of Rodolfo (1969a) which show 70 – 80% smectite in the WAS. Another possible reason for this increase is the smaller particle size of smectite which tends to be transported to distal areas from the source areas, compared to other clay minerals, thereby increasing its relative concentration in the deep seas (Kolla et al., 1976; Thiry, 2000). The La – Th – Sc ternary (**Fig. 6**) and La/Sc vs. Th/Sc (**Fig. 7**) plots also show the contribution from non – Irrawaddy sources to our study area. While the Irrawaddy River sediments are derived from the active and passive continental margin settings, the GC 3A sediments draw their source from the continental island arc settings (**Fig. 6**). The $Al_2O_3 - (CaO^* + Na_2O) - K_2O$ (A-CN-K) ternary diagram (Nesbitt and Young, 1984) also hints at a considerable contribution from sources with high degree of weathering to the GC 3A site. The GC 3A sediment data plot very close to the Andaman Flysch rocks and IBR rocks and away from the Irrawaddy River sediment data (**Fig. 6**).

To further decipher the potential sediment sources to WAS, published ϵ_{Nd} values from the Andaman Sea (taken from Colin et al., 1999; Awasthi et al., 2014; Ali et al., 2015; Damodararao et al., 2016; Miriyala et al., 2017) are compiled and a distribution map is prepared (**Fig. 8**). The map illustrates the high radiogenic nature of the WAS sediments compared to the EAS sediments. The ϵ_{Nd} value of the Irrawaddy River sediments ranges between -10.7 (Colin et al., 1999) and -8.3 (Allen et al., 2008) while the value of sediments from Barren Island is $+5.2$ (Luhr and Haldar, 2006). The low radiogenic ϵ_{Nd} values along with other geochemical and geophysical data (Kamesh Raju et al., 2004; Cao et al., 2015; Damodararao et al., 2016) of the Eastern Andaman Sea affirm the ISS source to the sediments in this area. But ϵ_{Nd} values in our core location (average ϵ_{Nd} for last 56 kyr = -6.2 , NGHP

01- 17A, Ali et al., 2015) are more radiogenic compared to the Eastern Andaman Sea suggesting a considerable contribution from high radiogenic sources to our study area.

The possible sources of high radiogenic sediments in our study area are the Indo -Burman - Arakan (IBA) ranges, volcanic rocks of Andaman Islands and the Barren volcano. The western slopes of IBA ranges are composed of Cretaceous and Oligocene sedimentary shales hosting volcanic dykes and ophiolites (Bender, 1983). From the available data, the IBA ranges seem to be highly radiogenic ($\epsilon_{Nd} = -4$, Allen et al., 2008) compared to the central Myanmar basin. The Andaman–Nicobar Islands are part of a 5600 km long curvilinear belt of accretionary ridges and outer-arc islands associated with the subduction of Indo-Australian oceanic lithosphere below an overriding Eurasian Plate (Bandopadhyay and Carter, 2017). The major stratigraphic units in the AN islands are the Ophiolite group, Mithakhari group, Andaman Flysch group and the Archipelago group (Pal et al., 2003). The general lithology of these stratigraphic units can be described as metasediments and metabasics (Ophiolite group), volcanoclastic turbidites (Mithakhari group), siliciclastic turbidites (Andaman Flysch group) and siliciclastic carbonate sediments (Archipelago group) (Pal et al., 2003). The ϵ_{Nd} value for Mithakhari group is -1.25 ($N = 24$) and for Andaman Flysch group is $\epsilon_{Nd} = -9.9$ ($N = 7$) (Awasthi, 2012) indicating the high radiogenic nature of some of the Andaman island rocks. The geochemical data of GC 3A core fall close to Andaman Flysch group data in the A-CN-K, La-Th-Sc and La/Sc vs. Th/Sc plots (**Figs. 6, b & c & 7**) indicating possible additional input from the local sources to our site. But the absence of major rivers and the physiographic constrains can restrict the sediment supply from the Andaman Islands. In addition to this, the volcanic islands of the Narcondam and Barren can also contribute high radiogenic sediments to the study area, but is possibly limited to smaller geographical extent. The sediment core SK 234 – 60 from the WAS near the Barren Volcano ($12^{\circ}05'46''N$ and $94^{\circ}05'18''E$; water depth 2 km) records a ϵ_{Nd} value of -6.01 for the last 20 kyr (Awasthi et al., 2014) which is similar to the NGHP record ($\epsilon_{Nd} = -6.0$, Ali et al., 2015) pointing towards similar sources of sediments at both these locations. From their Sr and Nd isotopic record, Awasthi et al. (2014) proposed an IBA dominated provenance at the WAS since the beginning of MIS 2, compared to the Irrawaddy dominated provenance before MIS 2.

The ϵ_{Nd} distribution and the geochemical discrimination diagrams together suggest IBA dominated provenance for GC 3A sediments. The lack of geochemical and isotopic data of rivers flowing through the IBA Ranges and Myanmar is a limitation for the source area characterization. Geochemical data of a sediment sample from Myittha River (Garzanti et al., 2016), a tributary to the Irrawaddy, which drains the IBA ranges, was chosen to represent IBA due to the lack of other

available data. The Myittha River data fall close to the GC 3A sediments in A-CN-K, La-Th-Sc and La/Sc vs. Th/Sc diagrams (**Figs. 6 & 7**) indicating the similarity in the sediment source at both the locations. In addition to this, the sediment sample from the Arakan continental shelf (SK 175/03, Damodararao et al., 2016) also falls close to the GC 3A cluster in ternary diagrams and affirms the IBA contribution to our sampling site. The IBA ranges supply sediments to the western shelf of Myanmar through the smaller rivers Kaladan, Naf, Lemro, Mayuetc owing to the heavy rainfall it receives during the SW monsoon (as high as 1 m/month -Xie et al., 2006). The east flowing surface currents during the SW monsoon can transport these sediments to the WAS (Rizal et al., 2012, Awasthi et al., 2014). While the Irrawaddy River sediment geochemical data (Garzanti et al., 2016) is different, the data for sediments at Irrawaddy mouth on Myanmar shelf (SK 175/38, Miriyala et al., 2017) falls closer to the GC 3A cluster in La-Th-Sc, A-CN-K and La/Sc vs. Th/Sc plots (**Figs. 6 & 7**) indicating the mixing of sediments in the Myanmar shelf owing to the macrotidal conditions and strong monsoon currents (Ramaswamy et al., 2004). From the geochemical, clay mineralogical and isotopic data, it is evident that the GC 3A site is receiving sediments mainly from the IBA ranges (with a minor contribution from local sources) compared to the Irrawaddy dominated central and eastern Andaman Sea.

5.2. Changes in paleoclimate and its implications in weathering patterns

Relatively, higher values of the magnetic concentration parameters (χ_{LF} , χ_{ARM} , SIRM) are found during the cold events such as LGM, YD and H1 compared to warm periods with lower values and coarsening trend of magnetic grain size parameters ($\chi_{ARM}/SIRM$, $SIRM/\chi_{LF}$, χ_{ARM}/χ_{LF}) (**Fig. 4**). These variations in the sediments can arise from a number of reasons including the changes in the source area, diagenesis, modifications in the hydrography and sea level, changes in the physical versus chemical weathering intensity etc. (e.g., Colin et al., 1998). The GC 3A samples plot in a cluster with minimum spread in the geochemical discrimination diagrams (La-Th-Sc, A-CN-K and La/Sc vs. Th/Sc – **Figs. 6 & 7**) suggesting limited provenance changes during the period of deposition. Additionally, ϵ_{Nd} isotopic data of NGHP 01 – 17A (same location of GC 3A; Ali et al., 2015) are nearly uniform (-5.3 to -7.1) suggesting that the sediment source did not change significantly during the time period the core has covered. The down core data of environmental magnetic parameters do not show any indications of significant alteration by post-depositional/diagenetic changes. Therefore, we infer that the primary factor controlling the variations in the mineral magnetic parameters is the variation in the physical and chemical weathering intensities in the source regions.

The intensity of silicate weathering is mainly governed by the temperature and rainfall in the area. The magnetic grain size is highly sensitive to these environmental changes (Kissel et al., 2003). Many workers have successfully utilized it as a proxy to study the variations in the balance between chemical and physical weathering at the source and to track the monsoonal variations as the dry and colder climate favors the physical weathering of rocks while wet and warmer climate increases the rate of chemical weathering (e.g. Colin et al., 1998; Kissel et al., 2003). The fining of magnetic grain size (indicated by the high values of $\chi_{\text{ARM}}/\text{SIRM}$ and $\chi_{\text{ARM}}/\chi_{\text{LF}}$) during the deglacial and early–mid Holocene periods manifest the increase in summer monsoon rainfall and the associated intensification in chemical weathering during these periods. In contrast to this, the magnetic parameters display coarser grain size during the dry, cold periods YD, H1 and LGM indicating reduced ISM and increased physical weathering in the source regions.

From the environmental magnetic data (**Fig. 4**), it is clear that the intensity of chemical weathering gradually increased from the LGM through deglacial period to Bølling-Allerød (B/A) except at 16.7 ka. This is similar to the recent finding of chemical weathering intensification in Myanmar watersheds at 17 ka responding to the deglacial warming (Miriayala et al., 2017). A single spike in the magnetic parameters at 16.7 ka in our record is synchronous with H1 event and may indicate the increased physical weathering during this period. A sudden change in the magnetic parameters at YD indicates a transition from the dominance of chemical weathering to physical weathering in the source regions.

In the Holocene, the mineral magnetic parameters record an increase in chemical weathering intensity from 11 to 3.5 kyr. The magnetic grain size shows two episodes of fining during 10.5 – 8.5 kyr and 5 – 3.5 kyr compared to other periods in early to mid-Holocene indicating the intensified chemical weathering during these periods. In the late Holocene (3.5 – 0 kyr), grain size parameters show a coarsening trend implying a reduction in chemical weathering intensity. This is synchronous with reduced solar insolation and mean moisture content (**Fig. 10**), which are not favorable for chemical weathering. The changes in the balance between physical and chemical weathering are also evident in clay mineral assemblages which were used to reconstruct the weathering scenario. The ratios smectite/(illite+chlorite) ($S/(I+C)$) and kaolinite/illite (K/I) are used as proxies of the chemical weathering intensity (Colin et al., 1999; Liu et al., 2007). Kaolinite and smectite are found in soils characterized by a warm, humid climate, and thus their occurrence reflect a strong climatic dependence controlled by the intensity of continental hydrolysis (Chamley, 1989). Illite and chlorite, on the other hand, are used as denominators as these minerals are considered as mainly primary minerals and are derived from physical erosion or moderate chemical weathering

(Colin et al., 2006). The ratios show high values during the deglacial, early and mid-Holocene periods and low values during LGM and YD (**Fig. 9**). This is consistent with the findings of Colin et al., (1999) that the LGM period, both in Bay of Bengal and Andaman Sea are characterized by a decrease in the $S/(I+C)$ ratio, suggesting increased physical weathering. Thus, the increase (decrease) in $S/(I+C)$ and K/I during wetter (drier) periods in our record suggest an increase in chemical (physical) weathering intensity in the source regions. The $S/(I+C)$ and K/I ratios also exhibit a peak in their values during 11.8 – 11.3 kyr signaling a rapid increase in chemical weathering at the culmination of YD (**Fig. 9**). Although this peak is evident in the weathering proxies (**Fig. 8**, WIP and CIA – detailed in the following section) of GC 3A (this study) and SK 168 (Miriayala et al., 2017), it is not recorded in the GC 3A magnetic grain size proxies. We infer that the increase in summer monsoonal strength at the beginning of the deglacial and Holocene had facilitated favorable conditions for stronger chemical weathering in the source regions. The Chemical Index of Alteration (CIA) (Nesbitt and Young, 1982) and the Weathering Index of Parker (WIP) (Parker, 1970) are among the most used proxies to evaluate the chemical weathering intensity in the source areas. The CIA is defined as

$$CIA = Al_2O_3 / (Al_2O_3 + CaO^* + Na_2O + K_2O) \times 100 \quad (1)$$

(calculated in molecular proportions of elemental oxides, CaO^* refers to CaO content in the silicate fraction of the sample).

The WIP is defined as

$$WIP = (2Na_2O/0.35 + MgO/0.9 + 2K_2O/0.25 + CaO/0.7) \times 100 \quad (2)$$

In this study, the WIP is used as the geochemical proxy for the chemical weathering intensity as CIA was found to be grain-size dependent. GC 3A contains relatively high amounts of sand and silt (average – 12% and 30% respectively) and the CIA values increased with decreasing grain size while the WIP values were relatively stable. Considering that the grain size can alter the CIA values, Nesbitt and Young (1982) who have devised this formula has originally recommended its use only for mud grade rocks (lutites). The grain size dependence of CIA was reported from many studies (Xiong et al., 2010; Bahlburg and Dobrzinski, 2011; Zhou et al., 2015) and care must be exercised while using bulk sediment geochemistry to calculate CIA and interpret the chemical weathering intensity in the source regions. The WIP on the other hand, behaves independent of grain size variations and has been found to be most appropriate for application to weathering profiles on heterogeneous parent rock (e.g., Price and Velbel, 2003). The WIP data suggest intense chemical weathering during the deglacial, early and mid-Holocene, similar to the environmental magnetic and

clay mineralogical changes (**Fig. 9**). The CIA record from the Central Andaman Sea sediment core SK 168 – GC 01 matches well with the GC 3A weathering record indicating a similar weathering pattern in the source areas of Central Myanmar and the IBA Ranges. The S/(I+C) record of NGHP 17A core (Ali et al., 2015) is also shown for comparison although their age model and the higher sedimentation rate offsets the S/(I+C) peaks from the increased weathering periods of GC 3A.

4.3. Coherency of this study with other local and global records

The environmental magnetic, clay mineralogical and geochemical data of the sediment core SSK 50 – GC 3A, studied here, indicate a stronger ISM strength and increased chemical weathering during the deglacial (16 – 13 kyr), early Holocene (10.5 – 8.5 kyr) and mid-Holocene (5 – 3.5 kyr) periods while a weakening in ISM strength was observed during late Holocene (3.5 – 0 kyr), YD (12.9 – 11.7 kyr) and 20 - 16 kyr periods in the IBR. The YD period was marked by reduced ISM strength while it increased during the B/A. The available paleoclimate records from the Andaman Sea along with some global records are compiled in **Fig. 10**. In general, the environmental magnetic record of GC 3A is in agreement with the $\delta^{18}\text{O}$ of NGRIP (Andersen et al., 2004), Hulu and Dongee records (Wang et al., 2001; Yuan et al., 2004). The ISM intensity recorded by the magnetic parameters is in tune with the sea surface temperature (SST) (RC 12-344; Rashid et al., 2007), Ba/Ca (Gebregiorgis et al., 2016) and $\delta^{18}\text{O}$ (SK 168; Sijin Kumar, 2011) records from the Andaman Sea and sea surface salinity (SSS) record from the Bay of Bengal (SO93-126KL in the northern Bay of Bengal, Kudrass et al., 2001). The SST and SSS records show enhanced fresh water input during B/A and mid Holocene periods indicating the increased ISM strength while LGM and YD periods show reduced fresh water input and a decreased ISM strength.

The mineral magnetic record of GC 3A suggests that the deglacial intensification of the ISM in the Myanmar region started at 16 ka and continued through B/A period. This is also evident from the increase in $\delta^{18}\text{O}$ records from this region and the decrease in SSS record from the nearby Bay of Bengal indicating the increased fresh water input. This warming trend and the ISM intensification were disrupted during the YD period. The ISM strength weakened during YD owing to the weakened Atlantic Meridional Overturning Circulation (AMOC), moderate negative radiative forcing and an altered atmospheric circulation (Renssen et al., 2015). The reduced ISM intensity in magnetic record during YD is in tune with the reduced mean effective moisture record over Asia (Herzschuh, 2006) and the salinity and oxygen isotope changes in the area (Kudrass et al., 2001; Rashid et al., 2007). The magnetic grain size parameters indicate that the abrupt cooling during the YD came to an end at 11.5 ka and the ISM strength increased gradually from there onwards. The

strong solar insolation during the early Holocene possibly caused an enhanced low-level convergence over the Tibetan Plateau thereby causing an intensification of summer monsoon rainfall (Herzschuh, 2006). The high sedimentation rate (9.4 cm/kyr) during the early Holocene in GC 3A record compared to other periods also indicates the increased terrigenous input from the source regions. This is consistent with the strengthened early Holocene monsoon induced massive sediment influx to the Ganges-Brahmaputra Delta too (Karpytchev et al., 2018). A gradual weakening in the ISM strength since the mid-Holocene (~4.5 ka) is seen which corresponds well with the lowered solar insolation and moisture record during this interval (**Fig. 10**). This late Holocene decrease in ISM intensity is consistent with other Andaman Sea records (Rashid et al., 2007; Achyuthan et al., 2014; Cao et al., 2015) and also in tune with the SSS record from the Bay of Bengal (Kudrass et al., 2001). Substantial aridification in the Indian Core Monsoon Zone (CMZ, east-central India) was also inferred between 4 and 1.7 kyr (Ponton et al., 2012) from the carbon isotopes of sedimentary leaf wax and oxygen isotope data of planktic foraminifera.

The millennial to centennial- scale variability of the ISM has been attributed to the solar activity (Agnihotri et al., 2002; Kodera, 2004; Gupta et al., 2005) and the changes in deep water formations in the North Atlantic (Altabet et al., 2002; Sinha et al., 2005). The solar influence on the Intertropical Convergence Zone (ITCZ) which controls the ISM is used to explain the Sun – monsoon link (Kodera, 2004). The ISM variability recorded by the mineral magnetic and geochemical proxies from GC 3A correlate well with the orbitally induced summer insolation changes indicating that the solar forcing is the main driver of ISM variability. In addition to this, the North Atlantic atmospheric teleconnection (e.g., Sijinkumar et al., 2016b) also does influence the ISM as evidenced from the presence of abrupt events YD and B/A in the sediment record.

6. Conclusions

A 21 kyr environmental magnetic and sediment geochemical record from the Western Andaman Sea tracks the provenance, weathering and monsoonal history in the Indo-Burman ranges of Myanmar. The results indicate that the sediments in the WAS received a considerable contribution from the IBR and local volcanic sources. The magnetic grain size changes track the changes in increased chemical weathering and Indian summer monsoon rainfall during the late glacial, early Holocene and mid-Holocene periods. The results also reveal that the Younger Dryas and the late Holocene periods witness reduced chemical weathering and ISM. The comparison of mineral magnetic parameters with global and local paleoclimate records show good coherency and illustrates the role of solar forcing on the ISM variability.

Acknowledgments

Authors are thankful to the Directors of CSIR - NIO, Goa and CSIR – NGRI, Hyderabad for providing the analytical facilities and support. Drs. A.V.Mudholkar, G.Parthiban, C.Prakash Babu and Pratima Kesarkar are gratefully acknowledged for providing the analytical facilities. Dr. N. Ramesh Babu, Mrs. Rupali Mohanty, Mr. Shemil Babu and Mr. Ashton Robinson Estibeiro are thanked for their help in environmental magnetic and major element measurements. Thanks are due to both the reviewers for their positive and helpful comments which helped improve the manuscript and colleague Dr. S.D.Iyer for sparing his time in improving the readability of the paper. We thank Ship Cell, NIO and the crew members of RV Sindhu Sankalp for helping us collect the sediment core used in this study. TS is thankful to CSIR—Shyama Prasad Mukherjee Fellowship (SPMF) for providing the research fellowship. This work is a contribution to CSIR XII Plan projects GEOSINKS (PSC0106) and GENIAS (PSC0104). This is CSIR - NIO's contribution No.XXXX.

References

- Achyuthan, H., Nagasundaram, M., Gourlan, A.T., Eastoe, C., Ahmad, S.M., Padmakumari, V.M., 2014. Mid-Holocene Indian Summer Monsoon variability off the Andaman Islands, Bay of Bengal. *Quat. Int.* 349, 232–244. <https://doi.org/10.1016/J.QUAINT.2014.07.041>
- Agnihotri, R., Dutta, K., Bhushan, R., Somayajulu, B.L., 2002. Evidence for solar forcing on the Indian monsoon during the last millennium. *Earth Planet. Sci. Lett.* 198, 521–527. [https://doi.org/10.1016/S0012-821X\(02\)00530-7](https://doi.org/10.1016/S0012-821X(02)00530-7)
- Ahmad, S.M., Patil, D.J., Rao, P.S., Nath, B.N., Rao, B.R., Rajagopalan, G., 2000. Glacial-interglacial changes in the surface water characteristics of the Andaman Sea: Evidence from stable isotopic ratios of planktonic foraminifera. *J. Earth Syst. Sci.* 109, 153–156. <https://doi.org/10.1007/BF02719159>
- Ali, S., Hathorne, E.C., Frank, M., Gebregiorgis, D., Statterger, K., Stumpf, R., Kutterolf, S., Johnson, J.E., Giosan, L., 2015. South Asian monsoon history over the past 60 kyr recorded by radiogenic isotopes and clay mineral assemblages in the Andaman Sea. *Geochemistry, Geophys. Geosystems* 16, 505–521. <https://doi.org/10.1002/2014GC005586>
- Allen, R., Carter, A., Najman, Y., Bandopadhyay, P.C., Chapman, H.J., Bickle, M.J., Garzanti, E., Vezzoli, G., Andò, S., Foster, G.L., Gerring, C., 2008a. New constraints on the sedimentation and uplift history of the Andaman-Nicobar accretionary prism, South Andaman Island, in: *Special Paper 436: Formation and Applications of the Sedimentary Record in Arc Collision Zones*. Geological Society of America, pp. 223–255. [https://doi.org/10.1130/2008.2436\(11\)](https://doi.org/10.1130/2008.2436(11))
- Allen, R., Najman, Y., Carter, A., Barfod, D., Bickle, M.J., Chapman, H.J., Garzanti, E., Vezzoli, G., Ando, S., Parish, R.R., 2008b. Provenance of the Tertiary sedimentary rocks of the Indo-Burman Ranges, Burma (Myanmar): Burman arc or Himalayan-derived? *J. Geol. Soc. London.* 165, 1045–1057. <https://doi.org/10.1144/0016-76492007-143>
- Altabet, M.A., Higginson, M.J., Murray, D.W., 2002. The effect of millennial-scale changes in

Arabian Sea denitrification on atmospheric CO₂. *Nature* 415, 159–162.
<https://doi.org/10.1038/415159a>

Andersen, K.K., Azuma, N., Barnola, J.-M., Bigler, M., Biscaye, P., Caillon, N., Chappellaz, J., Clausen, H.B., Dahl-Jensen, D., Fischer, H., Flückiger, J., Fritzsche, D., Fujii, Y., Goto-Azuma, K., Grønvold, K., Gundestrup, N.S., Hansson, M., Huber, C., Hvidberg, C.S., Johnsen, S.J., Jonsell, U., Jouzel, J., Kipfstuhl, S., Landais, A., Leuenberger, M., Lorrain, R., Masson-Delmotte, V., Miller, H., Motoyama, H., Narita, H., Popp, T., Rasmussen, S.O., Raynaud, D., Rothlisberger, R., Ruth, U., Samyn, D., Schwander, J., Shoji, H., Siggard-Andersen, M.-L., Steffensen, J.P., Stocker, T., Sveinbjörnsdóttir, A.E., Svensson, A., Takata, M., Tison, J.-L., Thorsteinsson, T., Watanabe, O., Wilhelms, F., White, J.W.C., White, J.W.C., 2004. High-resolution record of Northern Hemisphere climate extending into the last interglacial period. *Nature* 431, 147–151. <https://doi.org/10.1038/nature02805>

Awasthi, N., 2012. Geochemical and isotopic studies of sediments from the Andaman Islands and the Andaman sea. Maharaja Sayajirao University of Baroda.

Awasthi, N., Ray, J.S., Singh, A.K., Band, S.T., Rai, V.K., 2014. Provenance of the Late Quaternary sediments in the Andaman Sea: Implications for monsoon variability and ocean circulation. *Geochemistry, Geophys. Geosystems* 15, 3890–3906. <https://doi.org/10.1002/2014GC005462>

Babu, V.R., Sastry, J.S., 1976. Hydrography of the Andaman Sea During Late Winter. *Indian J. Mar. Sci.* 5, 179–189.

Bahlburg, H., Dobrzinski, N., 2011. A review of the Chemical Index of Alteration (CIA) and its application to the study of Neoproterozoic glacial deposits and climate transitions, in: *The Geological Record of Neoproterozoic Glaciations*. Geological Society of London, pp. 81–92. <https://doi.org/10.1144/M36.6>

Bandopadhyay, P.C., Carter, A., 2017. Geological framework of the Andaman–Nicobar Islands, in: Bandopadhyay, P.C., Carter, A. (Eds.), *Geological Society, London, Memoirs*. Geological Society of London, pp. 75–93. <https://doi.org/10.1144/M47.6>

Bender, F. (Friedrich), 1983. *Geology of Burma*. Gebr. Borntraeger.

Berger, A.L., 1978. Long-Term Variations of Daily Insolation and Quaternary Climatic Changes. *J. Atmos. Sci.* 35, 2362–2367. [https://doi.org/10.1175/1520-0469\(1978\)035<2362:LTVODI>2.0.CO;2](https://doi.org/10.1175/1520-0469(1978)035<2362:LTVODI>2.0.CO;2)

Biscaye, P., 1965. Mineralogy and Sedimentation of Recent Deep-Sea Clay in the Atlantic Ocean and Adjacent Seas and Oceans. *GSA Bull.* 76, 803–832. [https://doi.org/10.1130/0016-7606\(1965\)76\[803:masord\]2.0.co;2](https://doi.org/10.1130/0016-7606(1965)76[803:masord]2.0.co;2)

Bunsomboonsakul, S., Liu, Z., Sompongchaiyakul, P., Snidvongs, A., Krastel, S., 2012. Clay Mineralogical Records in Sediments along the Shelf Break of the Eastern Andaman Sea. *Am. Geophys. Union, Fall Meet. 2012*, Abstr. id. PP31C-2057.

Cao, P., Shi, X., Li, W., Liu, S., Yao, Z., Hu, L., Khokiattiwong, S., Kornkanitnan, N., 2015. Sedimentary responses to the Indian Summer Monsoon variations recorded in the southeastern Andaman Sea slope since 26ka. *J. Asian Earth Sci.* 114, 512–525. <https://doi.org/10.1016/j.jseaes.2015.06.028>

- Chamley, H., 1989. *Clay sedimentology*. Springer, Heidelberg.
- Clift, P.D., Hodges, K. V., Heslop, D., Hannigan, R., Van Long, H., Calves, G., 2008. Correlation of Himalayan exhumation rates and Asian monsoon intensity. *Nat. Geosci.* 1, 875–880. <https://doi.org/10.1038/ngeo351>
- Colin, C., Kissel, C.L., Blamart, D., Turpin, L., 1998. Magnetic properties of sediments in the Bay of Bengal and the Andaman Sea : impact of rapid North Atlantic Ocean climatic events on the strength of the Indian monsoon. *Earth Planet. Sci. Lett.* 160, 623–635.
- Colin, C., Turpin, L., Bertaux, J., Desprairies, A., Kissel, C., 1999. Erosional history of the Himalayan and Burman ranges during the last two glacial–interglacial cycles. *Earth Planet. Sci. Lett.* 171, 647–660. [https://doi.org/10.1016/S0012-821X\(99\)00184-3](https://doi.org/10.1016/S0012-821X(99)00184-3)
- Colin, C., Turpin, L., Blamart, D., Frank, N., Kissel, C., Duchamp, S., 2006. Evolution of weathering patterns in the Indo-Burman Ranges over the last 280 kyr: Effects of sediment provenance on $^{87}\text{Sr}/^{86}\text{Sr}$ ratios tracer. *Geochemistry, Geophys. Geosystems* 7. <https://doi.org/10.1029/2005GC000962>
- Collett, T.S., Riedel, M., Cochran, J.R., Boswell, R., Kumar, P., Sathe, A. V, 2008. Indian continental margin gas hydrate prospects: results of the indian national gas hydrate program (NGHP) expedition 01, in: *Proceedings of the 6th International Conference on Gas Hydrates (ICGH 2008)*.
- Curray, J.R., 2005. Tectonics and history of the Andaman Sea region. *J. Asian Earth Sci.* 25, 187–232. <https://doi.org/10.1016/J.JSEAES.2004.09.001>
- Damodararao, K., Singh, S.K., Rai, V.K., Ramaswamy, V., Rao, P.S., 2016. Lithology, Monsoon and Sea-Surface Current Control on Provenance, Dispersal and Deposition of Sediments over the Andaman Continental Shelf. *Front. Mar. Sci.* 3, 118. <https://doi.org/10.3389/fmars.2016.00118>
- Dearing, J.A., Bird, P.M., Dann, R.J.L., Benjamin, S.F., 1997. Secondary ferrimagnetic minerals in Welsh soils: a comparison of mineral magnetic detection methods and implications for mineral formation. *Geophys. J. Int.* 130, 727–736. <https://doi.org/10.1111/j.1365-246X.1997.tb01867.x>
- Duplessy, J.C., 1982. Glacial to interglacial contrasts in the northern Indian Ocean. *Nature* 295, 494–498. <https://doi.org/10.1038/295494a0>
- Garzanti, E., Wang, J.-G., Vezzoli, G., Limonta, M., 2016. Tracing provenance and sediment fluxes in the Irrawaddy River basin (Myanmar). *Chem. Geol.* 440, 73–90. <https://doi.org/10.1016/j.chemgeo.2016.06.010>
- Gebregiorgis, D., Hathorne, E.C., Sijinkumar, A.V., Nath, B.N., Nürnberg, D., Frank, M., 2016. South Asian summer monsoon variability during the last ~54 kyrs inferred from surface water salinity and river runoff proxies. *Quat. Sci. Rev.* 138, 6–15. <https://doi.org/10.1016/j.quascirev.2016.02.012>
- Gupta, A.K., Das, M., Anderson, D.M., 2005. Solar influence on the Indian summer monsoon during the Holocene. *Geophys. Res. Lett.* 32. <https://doi.org/10.1029/2005GL022685>
- Herzschuh, U., 2006. Palaeo-moisture evolution in monsoonal Central Asia during the last 50,000

years. *Quat. Sci. Rev.* 25, 163–178. <https://doi.org/10.1016/j.quascirev.2005.02.006>

- Kamesh Raju, K.A., Ramprasad, T., Rao, P.S., Ramalingeswara Rao, B., Varghese, J., 2004. New insights into the tectonic evolution of the Andaman basin, northeast Indian Ocean. *Earth Planet. Sci. Lett.* 221, 145–162. [https://doi.org/10.1016/S0012-821X\(04\)00075-5](https://doi.org/10.1016/S0012-821X(04)00075-5)
- Karpytchev, M., Ballu, V., Krien, Y., Becker, M., Goodbred, S., Spada, G., Calmant, S., Shum, C.K., Khan, Z., 2018. Contributions of a Strengthened Early Holocene Monsoon and Sediment Loading to Present-Day Subsidence of the Ganges-Brahmaputra Delta. *Geophys. Res. Lett.* 45, 1433–1442. <https://doi.org/10.1002/2017GL076388>
- Kissel, C., Laj, C., Clemens, S., Solheid, P., 2003. Magnetic signature of environmental changes in the last 1.2 Myr at ODP Site 1146, South China Sea. *Mar. Geol.* 201, 119–132. [https://doi.org/10.1016/S0025-3227\(03\)00212-3](https://doi.org/10.1016/S0025-3227(03)00212-3)
- Kodera, K., 2004. Solar influence on the Indian Ocean Monsoon through dynamical processes. *Geophys. Res. Lett.* 31, L24209. <https://doi.org/10.1029/2004GL020928>
- Kudrass, H.R.R., Hofmann, A., Dose, H., Emeis, K., Erlenkeuser, H., 2001. Modulation and amplification of climatic changes in the Northern Hemisphere by the Indian summer monsoon during the past 80 k.y. *Geology* 29, 63. [https://doi.org/10.1130/0091-7613\(2001\)029<0063:MAAOCC>2.0.CO;2](https://doi.org/10.1130/0091-7613(2001)029<0063:MAAOCC>2.0.CO;2)
- Kurian, S., Nath, B.N., Ramaswamy, V., Naman, D., Rao, T.G., Raju, K.A.K., Selvaraj, K., Chen, C.T.A., 2008. Possible detrital, diagenetic and hydrothermal sources for Holocene sediments of the Andaman backarc basin. *Mar. Geol.* 247, 178–193. <https://doi.org/10.1016/j.margeo.2007.09.006>
- Limmer, D.R., Bning, P., Giosan, L., Ponton, C., Köhler, C.M., Cooper, M.J., Tabrez, A.R., Clift, P.D., 2012. Geochemical record of Holocene to Recent sedimentation on the Western Indus continental shelf, Arabian Sea. *Geochemistry, Geophys. Geosystems* 13, 1–26. <https://doi.org/10.1029/2011GC003845>
- Liu, Z., Colin, C., Huang, W., Le, K.P., Tong, S., Chen, Z., Trentesaux, A., 2007. Climatic and tectonic controls on weathering in south China and Indochina Peninsula: Clay mineralogical and geochemical investigations from the Pearl, Red, and Mekong drainage basins. *Geochemistry, Geophys. Geosystems* 8, n/a-n/a. <https://doi.org/10.1029/2006GC001490>
- Luhr, J.F., Haldar, D., 2006. Barren Island Volcano (NE Indian Ocean): Island-arc high-alumina basalts produced by troctolite contamination. *J. Volcanol. Geotherm. Res.* 149, 177–212. <https://doi.org/10.1016/j.jvolgeores.2005.06.003>
- Miriyala, P., Sukumaran, N.P.P., Nath, B.N.N., Ramamurty, P.B.B., Sijinkumar, A.V. V., Vijayagopal, B., Ramaswamy, V., Sebastian, T., 2017. Increased chemical weathering during the deglacial to mid-Holocene summer monsoon intensification. *Sci. Rep.* 7, 44310. <https://doi.org/10.1038/srep44310>
- Naqvi, W.A., Charles, C.D., Fairbanks, R.G., 1994. Carbon and oxygen isotopic records of benthic foraminifera from the Northeast Indian Ocean: implications on glacial-interglacial atmospheric CO₂ changes. *Earth Planet. Sci. Lett.* 121, 99–110. [https://doi.org/10.1016/0012-821X\(94\)90034-5](https://doi.org/10.1016/0012-821X(94)90034-5)

- Nesbitt, H., Young, G., 1984. Prediction of some weathering trends of plutonic and volcanic rocks based on thermodynamic and kinetic considerations. *Geochim. Cosmochim. Acta* 48, 1523–1534. [https://doi.org/10.1016/0016-7037\(84\)90408-3](https://doi.org/10.1016/0016-7037(84)90408-3)
- Nesbitt, H.W., Young, G.M., 1982. Early Proterozoic climates and plate motions inferred from major element chemistry of lutites. *Nature* 299, 715–717. <https://doi.org/10.1038/299715a0>
- Pal, T., Chakraborty, P.P., Gupta, T.D., Singh, C.D., 2003. Geodynamic evolution of the outer-arcforearc belt in the Andaman Islands, the central part of the BurmaJava subduction complex. *Geol. Mag.* 140, S0016756803007805. <https://doi.org/10.1017/S0016756803007805>
- Parker, A., 1970. An Index of Weathering for Silicate Rocks. *Geol. Mag.* 107, 501. <https://doi.org/10.1017/S0016756800058581>
- Ponton, C., Giosan, L., Eglinton, T.I., Fuller, D.Q., Johnson, J.E., Kumar, P., Collett, T.S., 2012. Holocene aridification of India. *Geophys. Res. Lett.* 39, n/a-n/a. <https://doi.org/10.1029/2011GL050722>
- Potemra, J.T., Luther, M.E., O'Brien, J.J., 1991. The seasonal circulation of the upper ocean in the Bay of Bengal. *J. Geophys. Res.* 96, 12667. <https://doi.org/10.1029/91JC01045>
- Price, J.R., Velbel, M.A., 2003. Chemical weathering indices applied to weathering profiles developed on heterogeneous felsic metamorphic parent rocks. *Chem. Geol.* 202, 397–416. <https://doi.org/10.1016/J.CHEMGEO.2002.11.001>
- Rahaman, W., Singh, S.K., Sinha, R., Tandon, S.K., 2009. Climate control on erosion distribution over the Himalaya during the past ~100 ka. *Geology* 37, 559–562. <https://doi.org/10.1130/G25425A.1>
- Ramaswamy, V., Rao, P.S., Rao, K.H., Thwin, S., Srinivasa Rao, N., Raiker, V., 2004. Tidal influence on suspended sediment distribution and dispersal in the northern Andaman Sea and Gulf of Martaban. *Mar. Geol.* 208, 33–42. <https://doi.org/10.1016/j.margeo.2004.04.019>
- Rashid, H., Flower, B.P., Poore, R.Z., Quinn, T.M., 2007. A ~25ka Indian Ocean monsoon variability record from the Andaman Sea. *Quat. Sci. Rev.* 26, 2586–2597. <https://doi.org/10.1016/j.quascirev.2007.07.002>
- Renssen, H., Mairesse, A., Goosse, H., Mathiot, P., Heiri, O., Roche, D.M., Nisancioglu, K.H., Valdes, P.J., 2015. Multiple causes of the Younger Dryas cold period. *Nat. Geosci.* 8, 946–950. <https://doi.org/10.1038/NGEO2557>
- Rizal, S., Damm, P., Wahid, M.A., Sundermann, J., Ilhamsyah, Y., Iskandar, T., Muhammad, 2012. General circulation in the Malacca Strait and Andaman Sea: A numerical model study. *Am. J. Environ. Sci.* 8, 479–488.
- Robinson, R.A.J., Bird, M.I., Oo, N.W., Hoey, T.B., Aye, M.M., Higgitt, D.L., X. X., L., Swe, A., Tun, T., Win, S.L., 2007. The Irrawaddy River Sediment Flux to the Indian Ocean: The Original Nineteenth-Century Data Revisited. *J. Geol.* 115, 629–640. <https://doi.org/10.1086/521607>
- Rodolfo, K.S., 1969a. Sediments of the Andaman Basin, northeastern Indian Ocean. *Mar. Geol.* 7, 371–402. [https://doi.org/10.1016/0025-3227\(69\)90014-0](https://doi.org/10.1016/0025-3227(69)90014-0)

- Rodolfo, K.S., 1969b. Bathymetry and Marine Geology of the Andaman Basin, and Tectonic Implications for Southeast Asia. *Geol. Soc. Am. Bull.* 80, 1203. [https://doi.org/10.1130/0016-7606\(1969\)80\[1203:BAMGOT\]2.0.CO;2](https://doi.org/10.1130/0016-7606(1969)80[1203:BAMGOT]2.0.CO;2)
- Sebastian, T., Nath, B.N., Naik, S., Borole, D.V., Pierre, S., Yazing, A.K.A.K., 2017. Offshore sediments record the history of onshore iron ore mining in Goa State, India. *Mar. Pollut. Bull.* 114, 805–815.
- Sen Gupta, R., Moraes, C., George, M.D., Kureishy, T.W., Noronha, R.J., Fondecarr, S.P., 1981. Chemistry and Hydrography of the Andaman Sea. *Indian J. Mar. Sci.* 10, 228–233.
- Sijin Kumar, A., 2011. Paleooceanographic investigations of sediments from the Andaman sea. Goa University.
- Sijinkumar, A.V., Clemens, S., Nath, B.N., Prell, W., Benshila, R., Lengaigne, M., 2016a. $\delta^{18}\text{O}$ and salinity variability from the Last Glacial Maximum to Recent in the Bay of Bengal and Andaman Sea. *Quat. Sci. Rev.* 135, 79–91. <https://doi.org/10.1016/J.QUASCIREV.2016.01.022>
- Sijinkumar, A.V., Nagender Nath, B., Clemens, S., 2016b. North Atlantic climatic changes reflected in the Late Quaternary foraminiferal abundance record of the Andaman Sea, north-eastern Indian Ocean. *Palaeogeogr. Palaeoclimatol. Palaeoecol.* 446, 11–18. <https://doi.org/10.1016/J.PALAEO.2016.01.009>
- Sijinkumar, A.V., Nath, B.N., Guptha, M.V.S., 2010. Late Quaternary record of pteropod preservation from the Andaman Sea. *Mar. Geol.* 275, 221–229.
- Sinha, A., Cannariato, K.G., Stott, L.D., Li, H.-C., You, C.-F., Cheng, H., Edwards, R.L., Singh, I.B., 2005. Variability of Southwest Indian summer monsoon precipitation during the Bølling-Ållerød. *Geology* 33.1. <https://doi.org/10.1130/G21498.1>
- Thompson, R., Oldfield, F., 1986. *Environmental Magnetism*. Springer Netherlands, Dordrecht. <https://doi.org/10.1007/978-94-011-8036-8>
- Varkey, M.J., Murty, V.S.N., Suryanarayana, A., 1996. Physical oceanography of the Bay of Bengal and Andaman Sea. *Oceanogr. Mar. Biol. an Annu. Rev.* 34, 1–70.
- Wang, Y.J., Cheng, H., Edwards, R.L., An, Z.S., Wu, J.Y., Shen, C.C., Dorale, J.A., 2001. A high-resolution absolute-dated late Pleistocene Monsoon record from Hulu Cave, China. *Science* 294, 2345–8. <https://doi.org/10.1126/science.1064618>
- Wyrtki, K., 1973. *Physical Oceanography of the Indian Ocean*. Springer Berlin Heidelberg, pp. 18–36. https://doi.org/10.1007/978-3-642-65468-8_3
- Xie, S.-P., Xu, H., Saji, N.H., Wang, Y., Liu, W.T., Xie, S.-P., Xu, H., Saji, N.H., Wang, Y., Liu, W.T., 2006. Role of Narrow Mountains in Large-Scale Organization of Asian Monsoon Convection*. *J. Clim.* 19, 3420–3429. <https://doi.org/10.1175/JCLI3777.1>
- Xiong, S., Ding, Z., Zhu, Y., Zhou, R., Lu, H., 2010. A ~6 Ma chemical weathering history, the grain size dependence of chemical weathering intensity, and its implications for provenance change of the Chinese loess–red clay deposit. *Quat. Sci. Rev.* 29, 1911–1922. <https://doi.org/10.1016/j.quascirev.2010.04.009>

Yu, L., Oldfield, F., 1993. Quantitative sediment source ascription using magnetic measurements in a reservoir-catchment system near Nijar, S.E. Spain. *Earth Surf. Process. Landforms* 18, 441–454. <https://doi.org/10.1002/esp.3290180506>

Yuan, D., Cheng, H., Edwards, R.L., Dykoski, C.A., Kelly, M.J., Zhang, M., Qing, J., Lin, Y., Wang, Y., Wu, J., Dorale, J.A., An, Z., Cai, Y., 2004. Timing, duration, and transitions of the last interglacial Asian monsoon. *Science* 304, 575–8. <https://doi.org/10.1126/science.1091220>

Zhou, X., Li, A., Jiang, F., Lu, J., 2015. Effects of grain size distribution on mineralogical and chemical compositions: a case study from size-fractional sediments of the Huanghe (Yellow River) and Changjiang (Yangtze River). *Geol. J.* 50, 414–433. <https://doi.org/10.1002/gj.2546>

Figure Captions

Figure 1: Three dimensional map of the Andaman Sea depicting important rivers, volcanoes and other bathymetric features. The sampling locations of GC 3A core (this study in white) with other records (red) from the literature are also shown. Bathymetric data is taken from <https://maps.ngdc.noaa.gov/viewers/wcs-client>. The map was prepared in Golden Software Surfer with the perspective set to highlight the bathymetry (field of view 24° and tilt 43°) and therefore is not to the scale.

Figure 2: Calibrated radiocarbon dates versus core depth of GC 3A. The linear sedimentation rates for each interval are given.

Figure 3: Downcore variation of major clay minerals and texture in sediment core GC 3A. The 3 point running averages are plotted for clay mineralogy and D₅₀ (median size in micrometers) profiles.

Figure 4: Down core variation of CaCO₃, C_{org} and environmental magnetic parameters in core GC 3A indicating the concentration, grain size and mineralogy of the magnetic minerals. Major climatic events Younger Dryas (YD), Bølling-Allerød (B/A) and Last Glacial Maximum (LGM) are also shown.

Figure 5: Biplot of $\chi_{FD}\%$ versus $\chi_{ARM}/SIRM$ ratio indicating the magnetic grain size and the concentration of super paramagnetic (SP) grains.

Figure 6: Ternary diagrams showing the clay mineralogical and geochemical data of GC 3A in comparison to possible sources and other published work; (a) Clay mineralogy, (b) La-Th-Sc diagram, (c) Al₂O₃-CaO*+Na₂O-K₂O (A-CN-K) diagram. The references are given in the legend within the figure.

Figure 7: Biplot of La/Sc versus Th/Sc ratios of GC 3A sediments. Also plotted are the data of possible sources and other published work.

Figure 8: Regional variation of ϵ_{Nd} values in the Andaman Sea compiled from the literature (Colin et al., 1999; Awasthi et al., 2014; Ali et al., 2015; Damodararao et al., 2016; Miriyala et al., 2017). Exceptionally very high value of +5 (Barren island) is omitted for better representation. Our location (GC 3A) is same as that of NGHP-17 (white star) of Ali et al. (2015).

Figure 9: Comparison of environmental magnetic, geochemical and clay mineralogical indicators of weathering in core GC 3A core (a to e) compared with other Andaman Sea weathering records (f and g) of SK 168 – GC 01 (Miriya et.al., 2017) and NGHP 01 -17A (Ali et.al., 2015). (a) $\chi_{ARM}/SIRM$, (b) χ_{ARM}/χ_{LF} ; 3 point running averages of (c) Weathering Index of Parker (WIP), (d) kaolinite/illite ratio (K/I), (e) smectite/(illite + chlorite) (S/(I+C)) ratio; (f) Chemical Index of Alteration (CIA) of SK 168 – GC 01 and (g) S/(I+C) of NGHP 01 – 17A. The shaded areas mark the 3 chemical weathering events recorded in core GC 3A.

Figure 10: Comparison between the GC 3A magnetic record with the regional records of Indian summer monsoon variability and climatic parameters; (a) Summer solar insolation at 30°N (Berger, 1978), (b) Mean effective moisture of Asia (Herzschuh, 2006), (c) $\delta^{18}O$ record of NGRIP core (Andersen et al., 2004), (d) $\delta^{18}O$ record from Hulu and Dongee caves (Wang et al., 2001; Yuan et al., 2004), (e) $\delta^{18}O$ record of SK 168 - GC 01 (Sijin Kumar, 2011), (f) reconstructed sea surface temperature (SST) record of RC 12 - 344 (Rashid et al., 2007), (g) Sea surface salinity (SSS) record (126 KL) of Bay of Bengal (Kudrass et al., 2001), (h) Ba/Ca ratio of SK 168 – GC 01 (Gebregiorgis et al., 2016) and (i) $\chi_{ARM}/SIRM$ ratio of GC 3A. The shaded regions indicate the Last Glacial Maximum (LGM), Heinrich event 1 (H1) and Younger Dryas (YD).

Table 1: Major environmental magnetic parameters, their units and the description

Parameter	Units	Description
χ_{LF}	$10^{-8} \text{ m}^3 \text{ kg}^{-1}$	Low field susceptibility; indicator of magnetic mineral concentration in the sample
χ_{FD}	%	Frequency dependent susceptibility; $\chi_{FD} (\%) = [(\chi_{LF} - \chi_{HF}) / \chi_{LF}] \times 100$ (Mullins and Tite, 1973); Indicates the concentration of super paramagnetic (SP) grains.
χ_{ARM}	$10^{-5} \text{ m}^3 \text{ kg}^{-1}$	Susceptibility of anhysteretic remanent magnetization; Indicates the concentration of stable single domain (SSD) sized grains.
SIRM	$10^{-5} \text{ A m}^2 \text{ kg}^{-1}$	Saturation isothermal remanent magnetization; indicator of the concentration of remanent carrying magnetic minerals
χ_{ARM} / SIRM	10^{-5} m A^{-1}	Magnetic grain size indicator; higher (lower) values suggest a finer (coarser) magnetic grain size
χ_{ARM} / χ_{LF}	10^3	Magnetic grain size indicator; higher (lower) values suggest a finer (coarser) magnetic grain size
SIRM / χ_{LF}	10^3 A m^{-1}	Magnetic grain size indicator; higher (lower) values suggest a coarser (finer) magnetic grain size
Hard IRM	$10^{-5} \text{ A m}^2 \text{ kg}^{-1}$	Hard IRM = SIRM - IRM _{-300mT} ; indicator of the concentration of canted antiferromagnetic minerals such as hematite and goethite
S-ratio	Dimensionless	S-ratio = IRM _{-300mT} /SIRM; indicates the relative proportions of ferromagnetic and canted antiferromagnetic minerals; values close to 1 suggest a magnetite dominant mineralogy while values close to 0 suggest the dominance of hematite

Table 2: Table showing the accuracy and precision of major element data using X-Ray Fluorescence Spectrometry

Elemental Oxide		Al₂O₃	CaO	Na₂O	K₂O	MgO
JSO-1	Certified Value (wt.%)	17.99	2.56	0.66	0.34	2.11
	Obtained Value (wt.%)	16.88	2.67	0.64	0.34	1.92
JMS-1	Certified Value (wt.%)	15.82	2.13	4.07	2.24	2.87
	Obtained Value (wt.%)	15.60	2.11	4.07	2.23	2.83
MAG-1	Certified Value (wt.%)	16.40	1.37	3.83	3.55	3.00
	Obtained Value (wt.%)	16.05	1.40	3.76	3.60	2.94
Average Accuracy (%)		±2.5	±2.1	±1.8	±0.6	±3.0
Precision (%)		±0.1	±0.1	±1.4	±0.2	±0.2

Table 3: Table showing the accuracy and precision of trace element data using ICP-MS

Elemental Oxide		La	Sc	Th
JSD-1	Certified Value (ppm)	18.1	10.9	4.44
	Obtained Value (ppm)	18.23	10.75	4.441
	Accuracy (%)	±0.7	±1.4	±0.7
SGR-1b	Certified Value (ppm)	20	4.6	4.8
	Obtained Value (ppm)	20.15	4.907	4.799
	Accuracy (%)	±0.7	±6.7	±0.02
Sample	Precision (%) (average of all repeat measurements)	±2.368	±3.762	±4.14

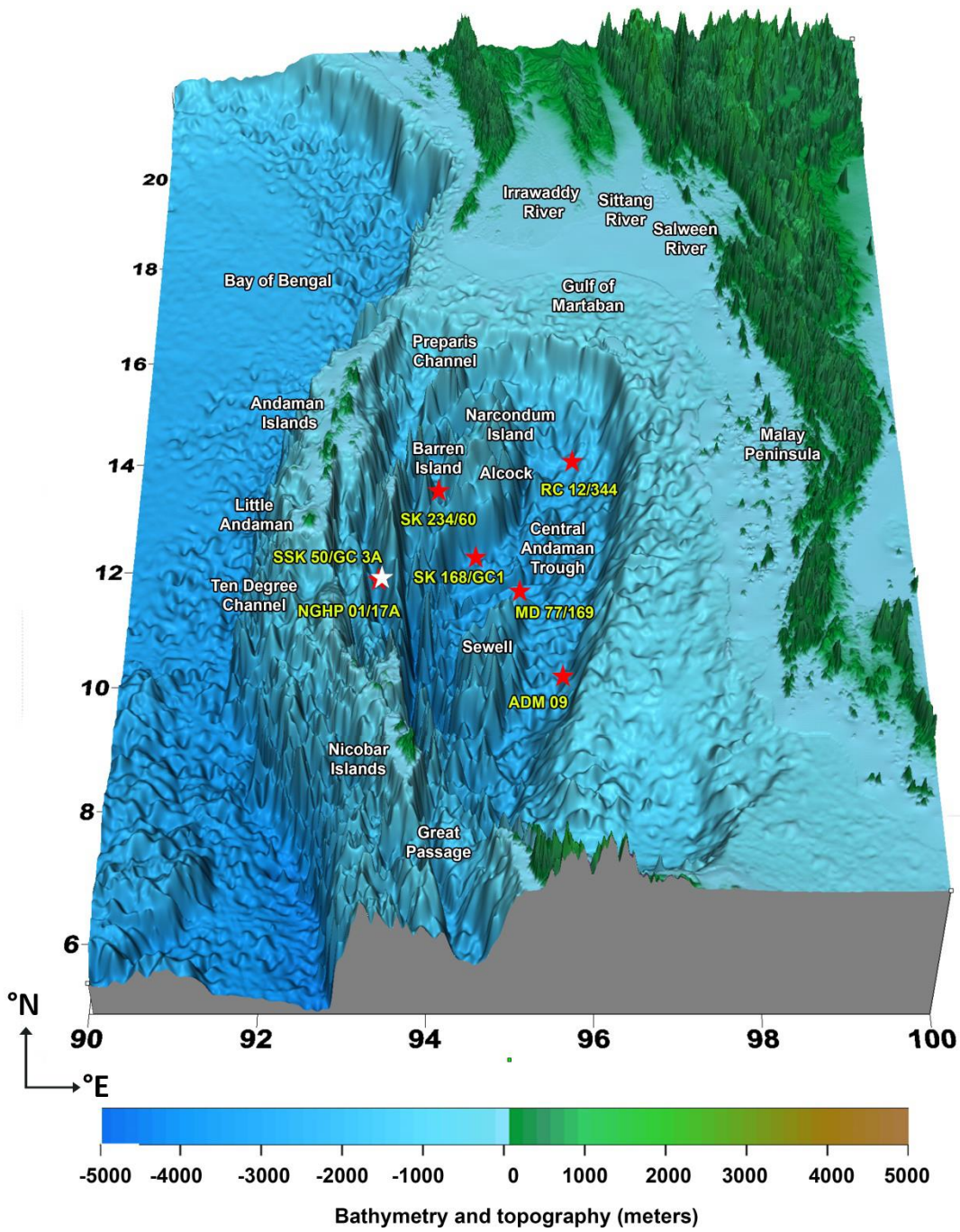


Figure 1

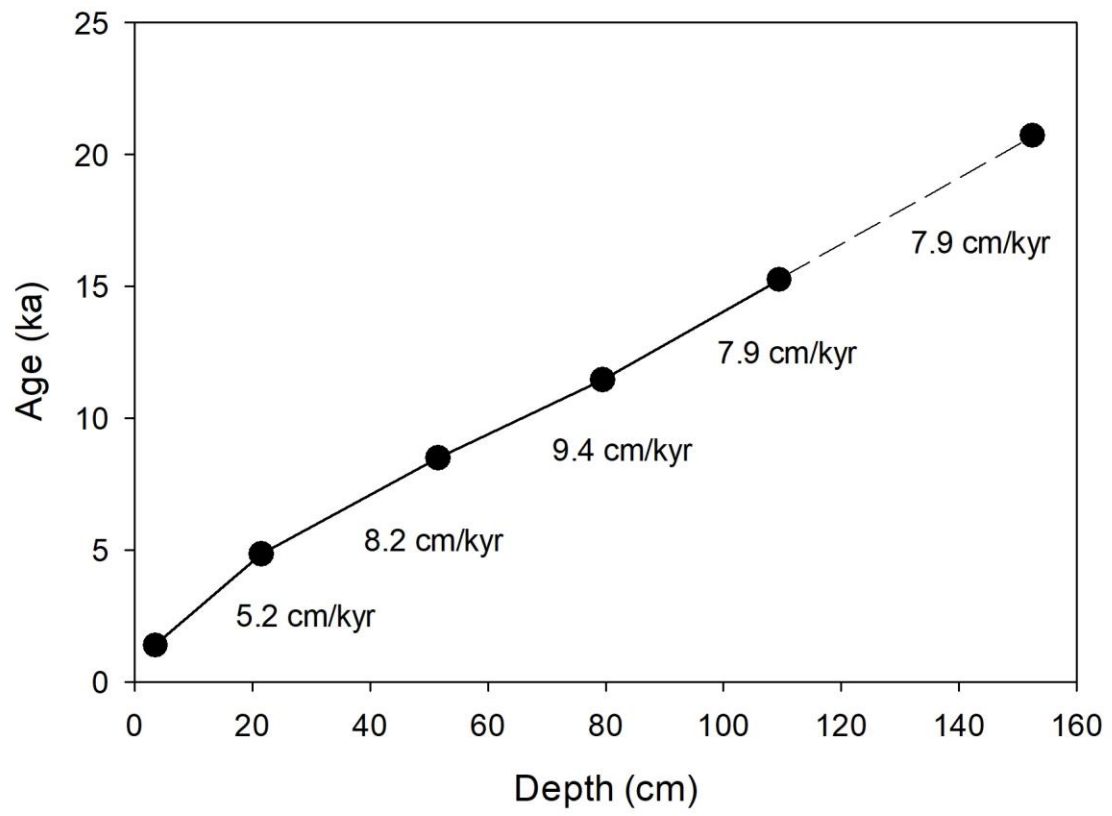
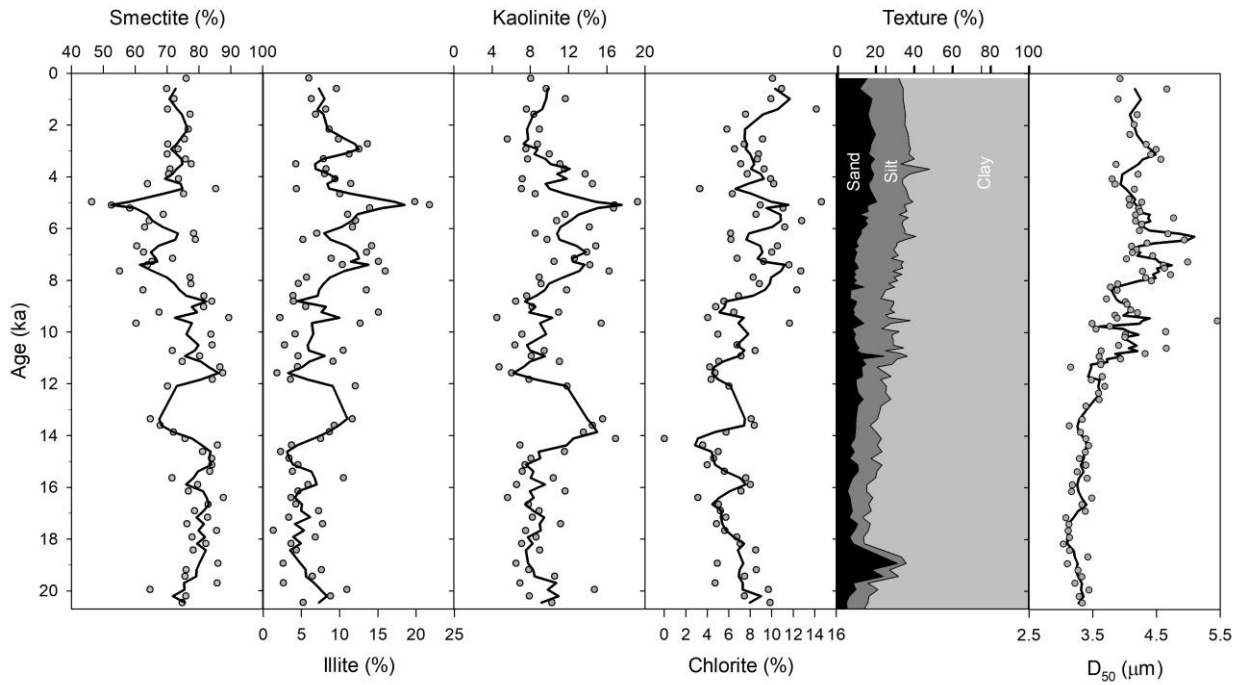


Figure 2

**Figure 3**

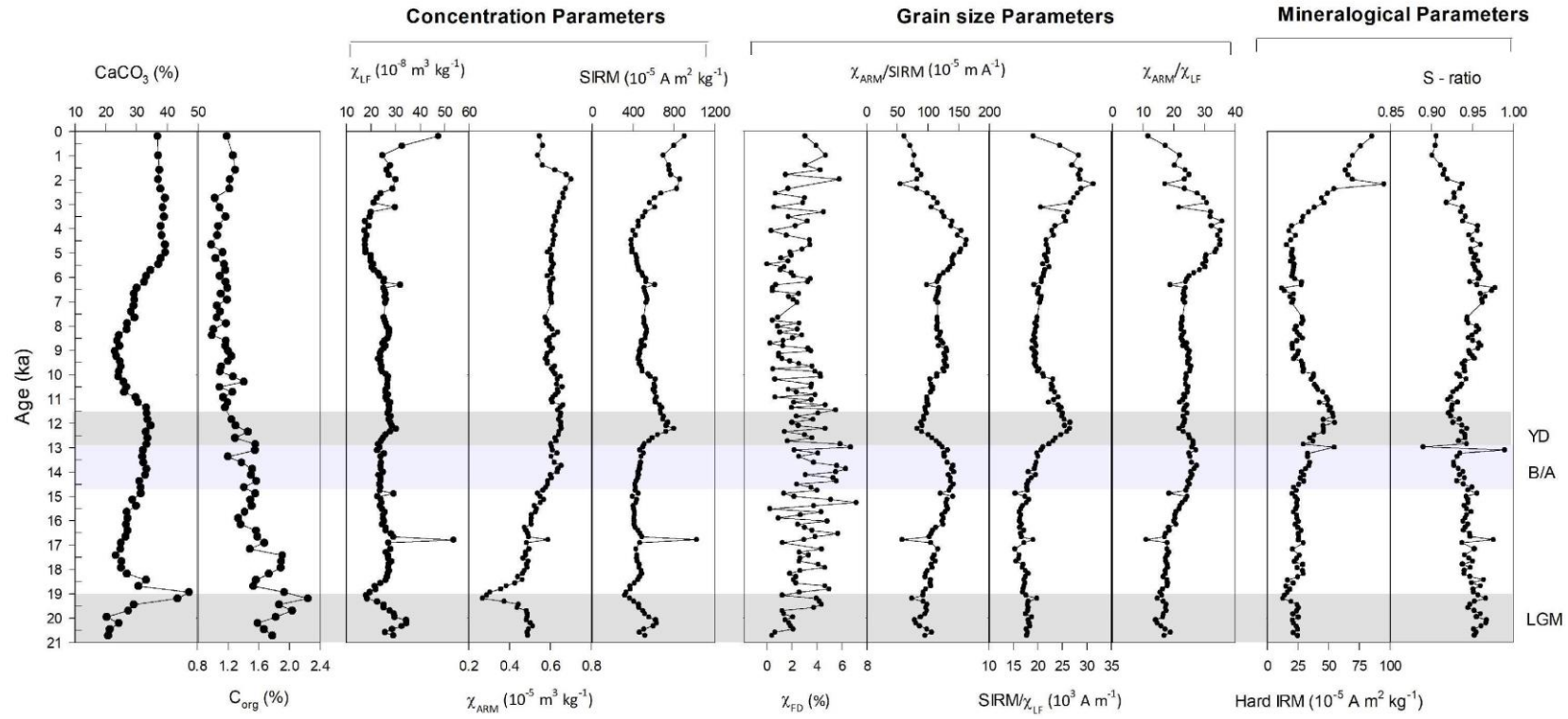
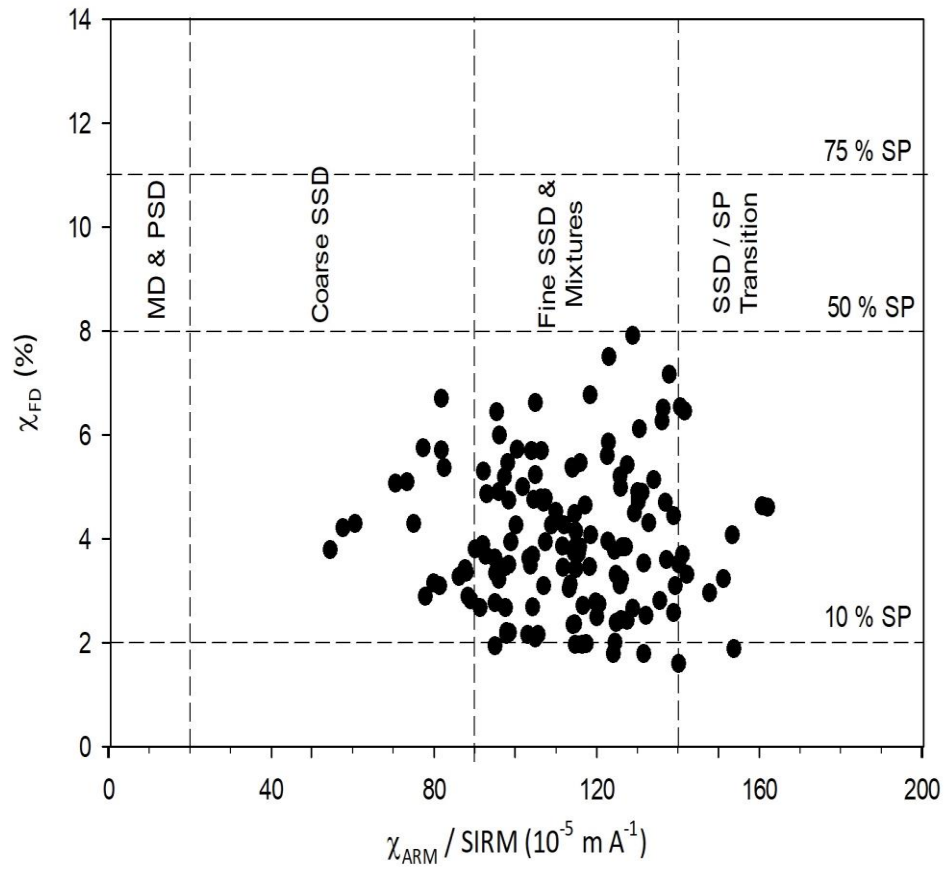
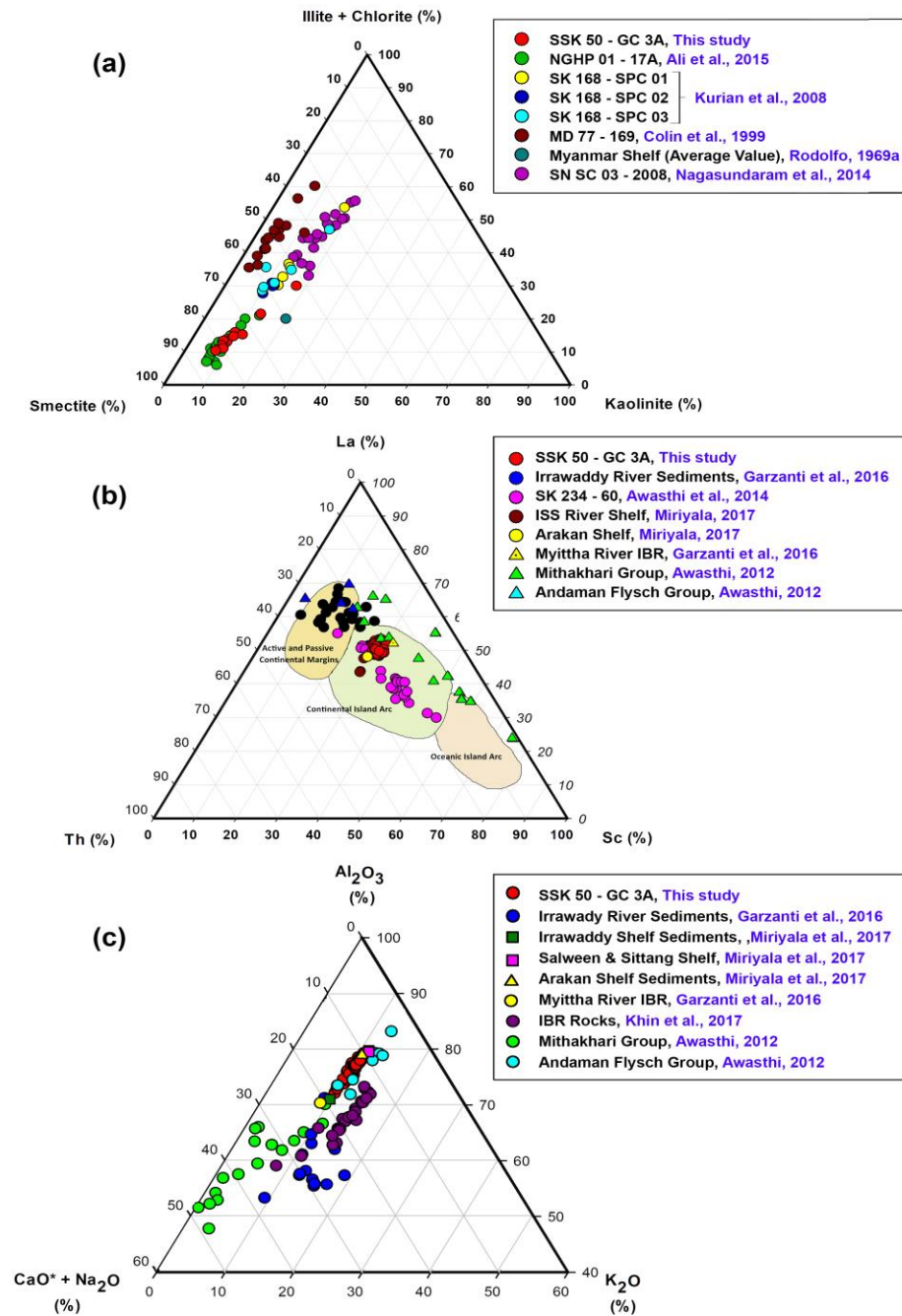


Figure 4

**Figure 5**



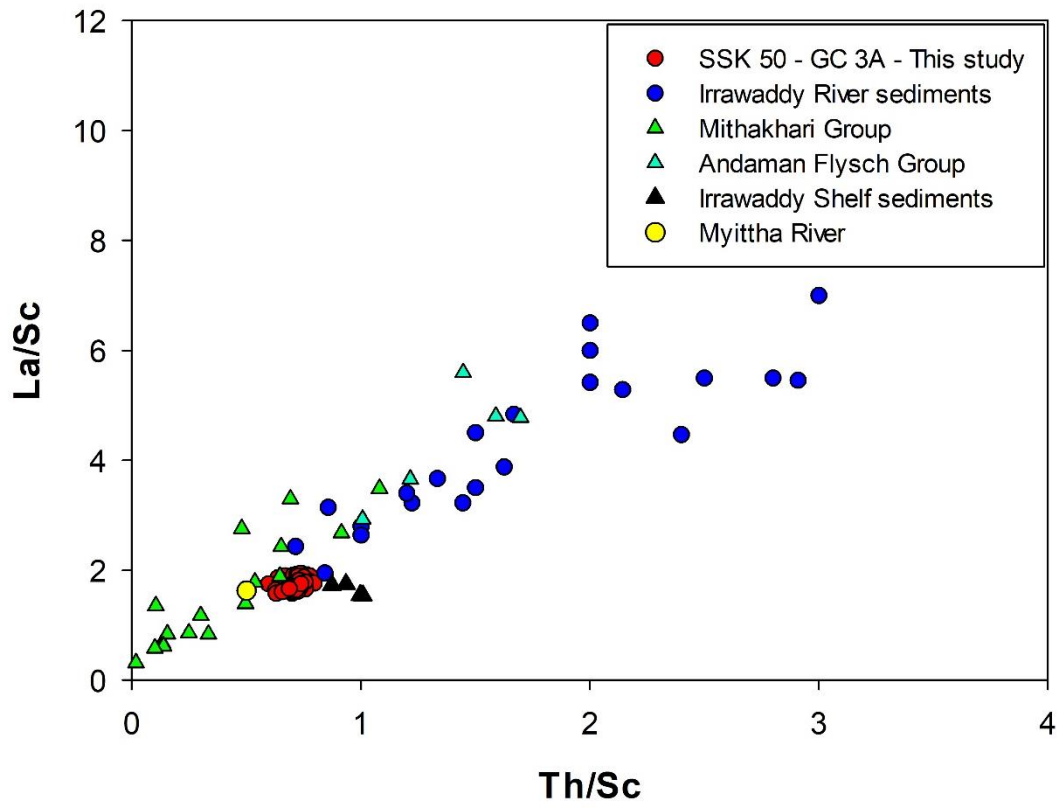


Figure 7

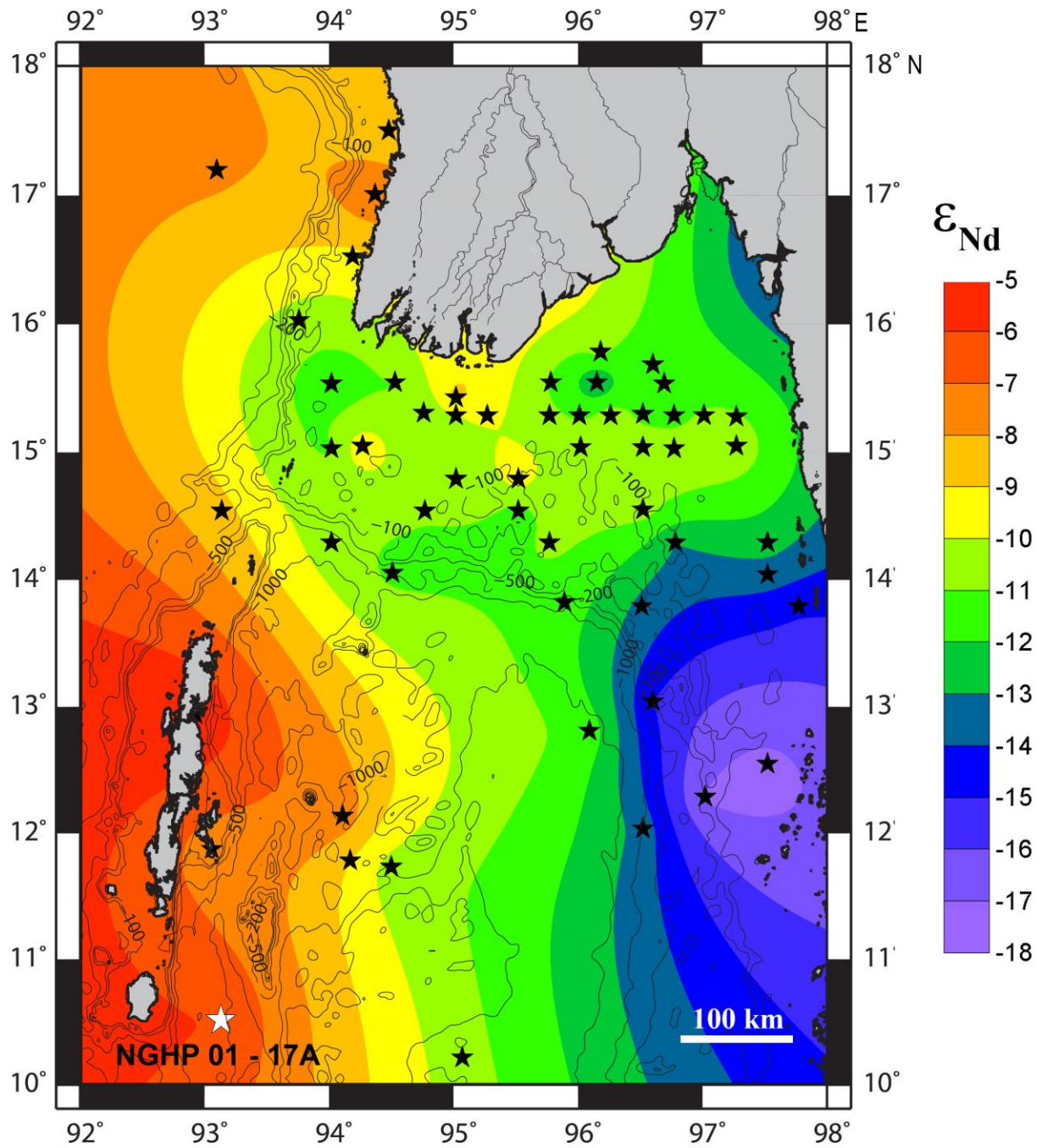


Figure 8

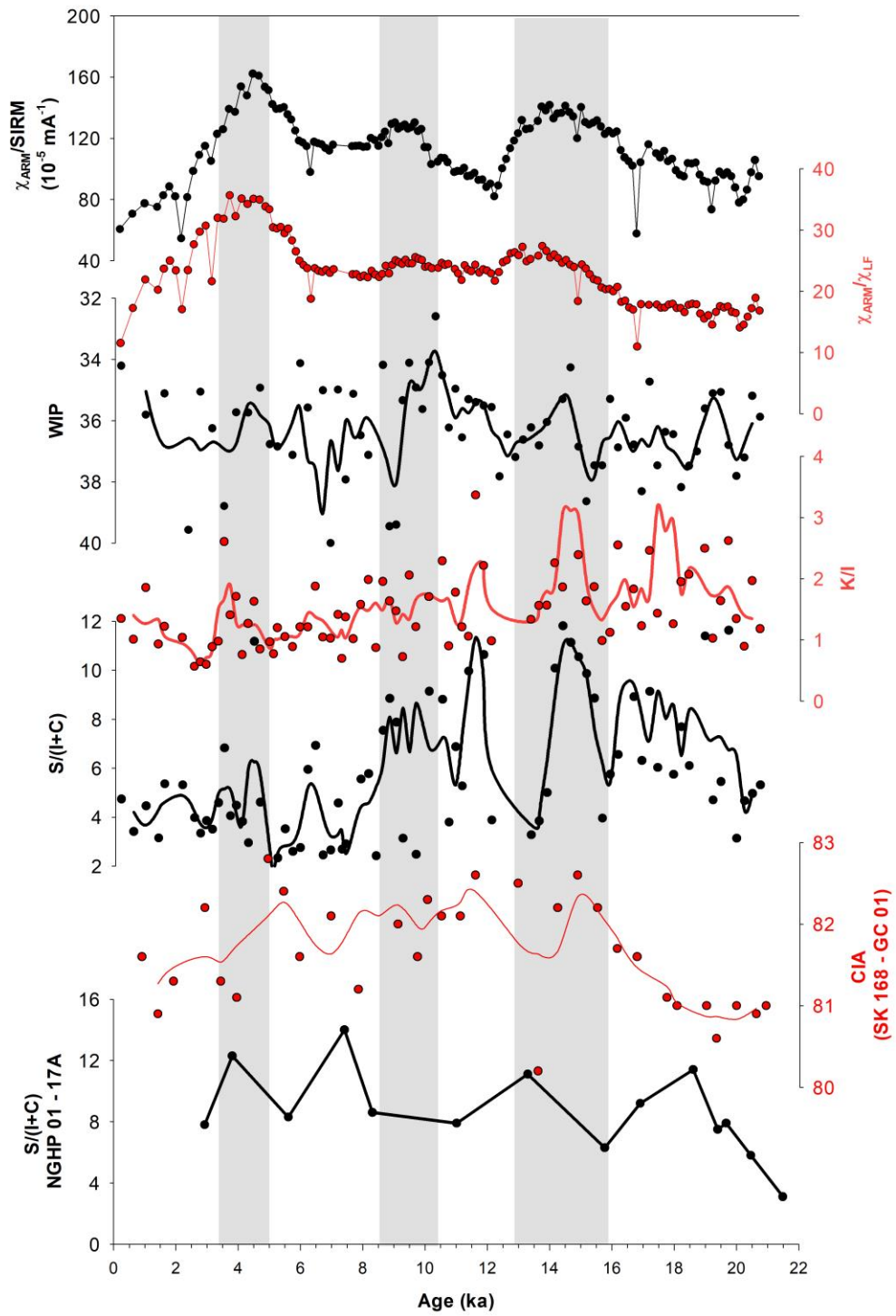


Figure 9

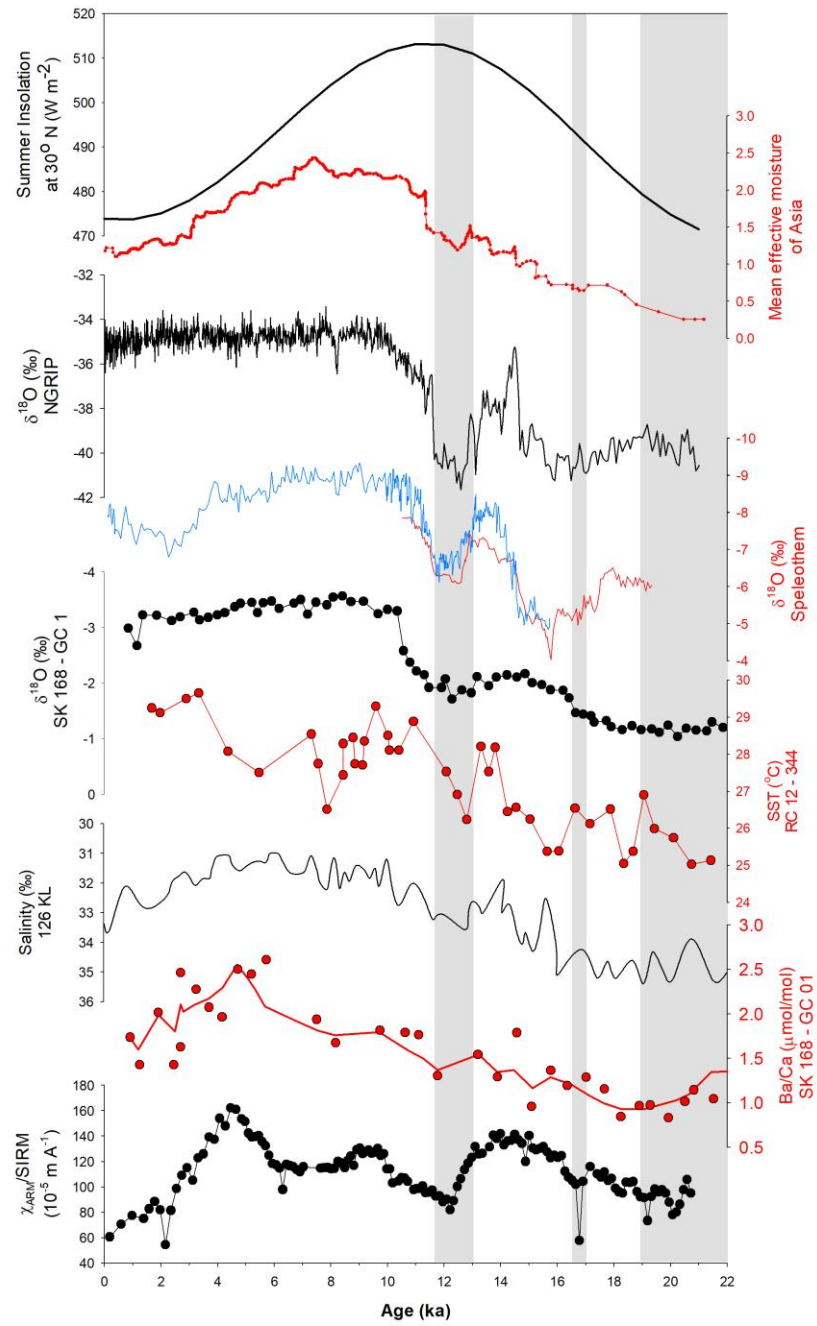


Figure 10